

PAPER • OPEN ACCESS

Fluid surface coatings for solid-state nanopores: comparison of phospholipid bilayers and archaea-inspired lipid monolayers

To cite this article: Olivia M Eggenberger *et al* 2019 *Nanotechnology* **30** 325504

View the [article online](#) for updates and enhancements.



IOP | ebooks™

Bringing you innovative digital publishing with leading voices to create your essential collection of books in STEM research.

Start exploring the collection - download the first chapter of every title for free.

Fluid surface coatings for solid-state nanopores: comparison of phospholipid bilayers and archaea-inspired lipid monolayers

Olivia M Eggenberger¹ , Geoffray Leriche², Takaoki Koyanagi²,
Cuifeng Ying¹ , Jared Houghtaling^{1,3} , Thomas B H Schroeder^{1,4},
Jerry Yang², Jiali Li⁵, Adam Hall⁶ and Michael Mayer^{1,3}

¹ Adolphe Merkle Institute, University of Fribourg, Fribourg, Switzerland

² Department of Chemistry and Biochemistry, University of California, San Diego, La Jolla, CA, United States of America

³ Department of Biomedical Engineering, University of Michigan, Ann Arbor, MI, United States of America

⁴ Department of Chemical Engineering, University of Michigan, Ann Arbor, MI, United States of America

⁵ Department of Physics, University of Arkansas, Fayetteville, AR, United States of America

⁶ Virginia Tech-Wake Forest University School of Biomedical Engineering and Sciences, Wake Forest School of Medicine, Winston-Salem, NC, United States of America

E-mail: michael.mayer@unifr.ch

Received 20 December 2018, revised 4 April 2019

Accepted for publication 16 April 2019

Published 16 May 2019



CrossMark

Abstract

In the context of sensing and characterizing single proteins with synthetic nanopores, lipid bilayer coatings provide at least four benefits: first, they minimize unwanted protein adhesion to the pore walls by exposing a zwitterionic, fluid surface. Second, they can slow down protein translocation and rotation by the opportunity to tether proteins with a lipid anchor to the fluid bilayer coating. Third, they provide the possibility to impart analyte specificity by including lipid anchors with a specific receptor or ligand in the coating. Fourth, they offer a method for tuning nanopore diameters by choice of the length of the lipid's acyl chains. The work presented here compares four properties of various lipid compositions with regard to their suitability as nanopore coatings for protein sensing experiments: (1) electrical noise during current recordings through solid-state nanopores before and after lipid coating, (2) long-term stability of the recorded current baseline and, by inference, of the coating, (3) viscosity of the coating as quantified by the lateral diffusion coefficient of lipids in the coating, and (4) the success rate of generating a suitable coating for quantitative nanopore-based resistive pulse recordings. We surveyed lipid coatings prepared from bolaamphiphilic, monolayer-forming lipids inspired by extremophile archaea and compared them to typical bilayer-forming phosphatidylcholine lipids containing various fractions of curvature-inducing lipids or cholesterol. We found that coatings from archaea-inspired lipids provide several advantages compared to conventional phospholipids; the stable, low noise baseline qualities and high viscosity make these membranes especially suitable for analysis that estimates physical protein parameters such as the net charge

 Original content from this work may be used under the terms of the [Creative Commons Attribution 3.0 licence](https://creativecommons.org/licenses/by/3.0/). Any further distribution of this work must maintain attribution to the author(s) and the title of the work, journal citation and DOI.

of proteins as they enable translocation events with sufficiently long duration to time-resolve dwell time distributions completely. The work presented here reveals that the ease or difficulty of coating a nanopore with lipid membranes did not depend significantly on the composition of the lipid mixture, but rather on the geometry and surface chemistry of the nanopore in the solid state substrate. In particular, annealing substrates containing the nanopore increased the success rate of generating stable lipid coatings.

Supplementary material for this article is available [online](#)

Keywords: nanopore, single protein, lipid coating, archaea-inspired lipids, stability, noise

(Some figures may appear in colour only in the online journal)

1. Introduction

1.1. Background

Nanopore-based resistive pulse recordings are emerging as a powerful single-molecule characterization approach with applications in nucleic acid sequencing [1–7], biomolecule detection [8–11], characterization of single proteins [12–17], and biomarker-based diagnostics [18]. For instance, we showed recently that solid-state nanopores whose walls are coated with a fluid lipid membrane make it possible to fingerprint proteins with regard to their volume, approximate shape, charge, dipole moment and rotational diffusion coefficient [15].

In nanopore-based single molecule characterization, a high-gain current amplifier applies a constant potential difference between two electrolyte compartments separated by a thin insulating membrane. The amplifier records the ionic current through a single, electrolyte-filled nanopore in the membrane that connects the two compartments. As non-conducting macromolecules transit the pore, they typically cause transient reductions in the ionic current that contain information about the volume, charge, shape, and dipole moment of the translocating species [15, 19–22].

The earliest and much of the recent work in nanopore sensing employed biological protein pores spanning a planar lipid bilayer [23, 24]. The dimensions of these pores are well defined and typically constant from one protein nanopore to the next, as long as the protein's amino acid sequence is not altered; in addition, protein pores often display minimal non-specific interactions with most analytes of interest [3, 25]. The diameters of the narrowest constriction of wildtype protein pores are, however, limited to a range between 0.4 and 3.3 nm, precluding the translocation of midsize and large proteins as well as other large analytes [2]. Recently, nanopores fabricated in synthetic substrates have enabled the analysis of larger particles [11, 26, 27], but surface interactions between these solid-state nanopores and biomolecules can result in undesired non-specific adsorption and clogging [16, 28, 29].

To reduce non-specific adsorption to the substrates of solid-state nanopores, various groups explored surface

treatments such as silanization [30–32], self-assembled monolayers of thiols on gold films [33–35], atomic layer deposition of metal oxides [36, 37], and surfactant coatings [38, 39]. Some of these coatings also functionalized the pore surface [14, 40, 41] to improve detection efficiency [13, 42, 43]. In 2011, our group introduced a fluid lipid membrane coating [16], which eliminated or minimized non-specific interactions with the pore walls and enabled conjugation of proteins to mobile lipid anchors in the membrane [16]. This lipid anchor strategy significantly slows the translocation speeds and rotational dynamics of tethered proteins while circumventing undesired non-specific interactions with nanopore walls [15]. Slow translocation speeds enable current recordings that resolve most translocation events fully in magnitude and time and yield a large amount of data from individual translocation events. Together, these benefits of long-lived translocation events bolster the information content and statistics from individual resistive pulses. The strategy of tethering proteins to lipid anchors therefore enables the characterization of individual proteins beyond the determination of their volume and translocation time [15]. In particular, by eliminating or minimizing non-specific interactions with the pore walls, lipid coatings make it possible to quantify and interpret translational and rotational dynamics of lipid-anchored proteins as they move through the nanopore [15]. This approach makes it possible to extract the protein's dipole moment, and rotational diffusion coefficient in addition to its shape and volume from an individual translocation event and is a first step towards identifying and counting individual proteins in mixtures [15]. While alternative nanopore coatings can also minimize clogging of nanopores and have the advantage that they are more straightforward to apply to the pore walls and chemically more robust than lipid coatings, their disadvantage is that they have not yet been able to minimize non-specific interactions to pore walls sufficiently to allow for the quantification of single molecule protein characteristics that rely on translocation and rotation, such as protein charge or dipole [35, 44]. Notably, the ability to anchor a protein to the bilayer allows for the determination of charge based on the distribution of translocation times for that protein [15, 16].

Here, we sought an ideal lipid-based surface coating that coats synthetic nanopores in silicon-nitride substrates in a straightforward and reproducible manner, while maintaining a stable and low-noise electrical baseline and slowing down the translational and rotational speed of non-spherical, lipid-anchored proteins such that orientation-dependent modulations in current during a translocation event could be resolved and quantified in time. In order to evaluate the quality and integrity of these bilayer coatings, we took advantage of measurements of protein charge. To do so, we recorded translocation time distributions of three lipid-anchored proteins and fit these distributions to the equation for biased first-passage time [45] with protein charge as a fitting parameter. Close agreement of the protein charge determined from the fit with the theoretically expected charge indicated that proteins translocated ideally and as theoretically predicted by the first-passage time equation; if non-specific interactions within the pore would have slowed down the proteins, then the translocation time could not be fitted well by the biased first-passage time equation and the determined protein charge would be significantly lower than expected.

1.2. Coating parameters

Applying a fluid lipid coating to a solid-state nanopore can increase the low frequency noise in current recordings, likely due to undulations of the coating [46]. As the ability to identify translocation events in a current recording is limited by the signal-to-noise ratio [47], an ideal nanopore coating would add minimal additional noise to the system or would even reduce the noise [16]. A coated nanopore must also yield a baseline current that varies minimally over various time scales, as fluctuations can lead to artifacts in the analysis.

The lateral diffusion coefficient (D_L) of lipids in a membrane is an important parameter in resistive pulse experiments that employ lipid-tethered analytes [16]. Yusko *et al* and Plesa *et al* demonstrated that only a small fraction of untethered proteins translocating through nanopores take sufficiently long to be time-resolved due to limitations of the recording bandwidth and the signal-to-noise ratio of the equipment [16, 48]. Proteins with lipid tethers that are anchored in a viscous lipid membrane coating, however, have more than 100-fold prolonged dwell times (t_d) in the pore compared to untethered proteins because the lateral diffusion coefficient of a tethered protein is dominated by the diffusion of its lipid anchor [16]. Slow protein movement is favorable since it increases the fraction of translocation events with dwell times longer than the time-resolution threshold of the recordings [16].

The work presented here, together with earlier work [15, 16, 49, 50], shows that nanopore fabrication methods and post fabrication processing steps affect the ease of coating a pore and the stability of the coating during nanopore experiments. In this paper, we coated pores that were made by three different fabrication techniques: ion-beam sculpting [7, 51], ion-beam drilling [52–54], and dielectric breakdown [50, 55]. A final goal of the work presented here was to identify the attributes of lipid coatings and pore fabrication

strategies that facilitate reproducible formation of membrane coatings.

1.3. Experimental design: lipids tested

Figure 1 shows the chemical structure of the different classes of lipids tested in this study. In an attempt to decrease noise levels and increase the overall stability of the coating, we added various proportions of cholesterol into bilayers of 1-palmitoyl-2-oleoyl-sn-glycero-3-phosphocholine (POPC). Cholesterol increases stability in lipid membranes [56] because of its effect on membrane structure and packing [57–59]. Additionally, membranes with increasing proportions of cholesterol are more viscous, with correspondingly reduced D_L values [16, 60]. Here, we hypothesized that increasing the cholesterol concentration in the coating would prolong protein dwell times and lead to coatings with good stability.

We also tested fluid lipid coatings inspired by extremophile organisms of the kingdom archaea, which often have cell membranes composed of bolaamphiphilic lipids [61, 62]. These lipid structures have two terminal polar head groups connected covalently by a hydrophobic alkyl chain and form lipid membranes composed of fluid monolayers instead of bilayers. These lipids are thought to stabilize cell membranes, allowing extremophiles to survive in environments with extreme temperature, pH and salinity [61, 62]. To test if coatings from these lipids would be beneficial, we coated nanopores with a class of chemically synthesized archaea-inspired bolaamphiphilic lipids containing two glycerophosphocholine heads, which were attached to glycerol by an ether-bond to one pendant phytanyl chain and to one end of a membrane-spanning hydrocarbon chain (figures 1(A)–(C)). We have recently examined the ion permeation kinetics of membranes composed of these lipids [63–67] and since we had a selection of these lipids available, we tested eight of them.

For comparison, we additionally tested coatings composed of two commercially available and widely used non-bolaform archaea-inspired lipids: 1,2-diphytanoyl-sn-glycero-3-phosphocholine (DiPhyPC) and 1,2-di-O-phytanoyl-sn-glycero-3-phosphocholine (Di-O-PhyPC).

Finally, we hypothesized that the discrepancy in ease of coating between different pores may be due to heterogeneities in the ‘sharpness’ of the radii of curvature of the corners at the brims of the pores. As we have reported previously, the success rate of forming a lipid coating on a nanopore chip can vary from 10% to 50% depending on the chip and we found that nanopores with diameters smaller than 17 nm [50] and pores with sharp edges of extreme curvature could, so far, not be coated with lipid membranes. Similar limitations of forming lipid membranes with extreme curvature have been reported for phospholipid vesicles [68] and for lipid coatings of nanoparticles [69–71]. We therefore tested if lipid membrane compositions that form more flexible coatings with regard to membrane curvature, when compared to those composed of cylindrically shaped lipids, would be able to conform more readily to sharp corners and thereby coat

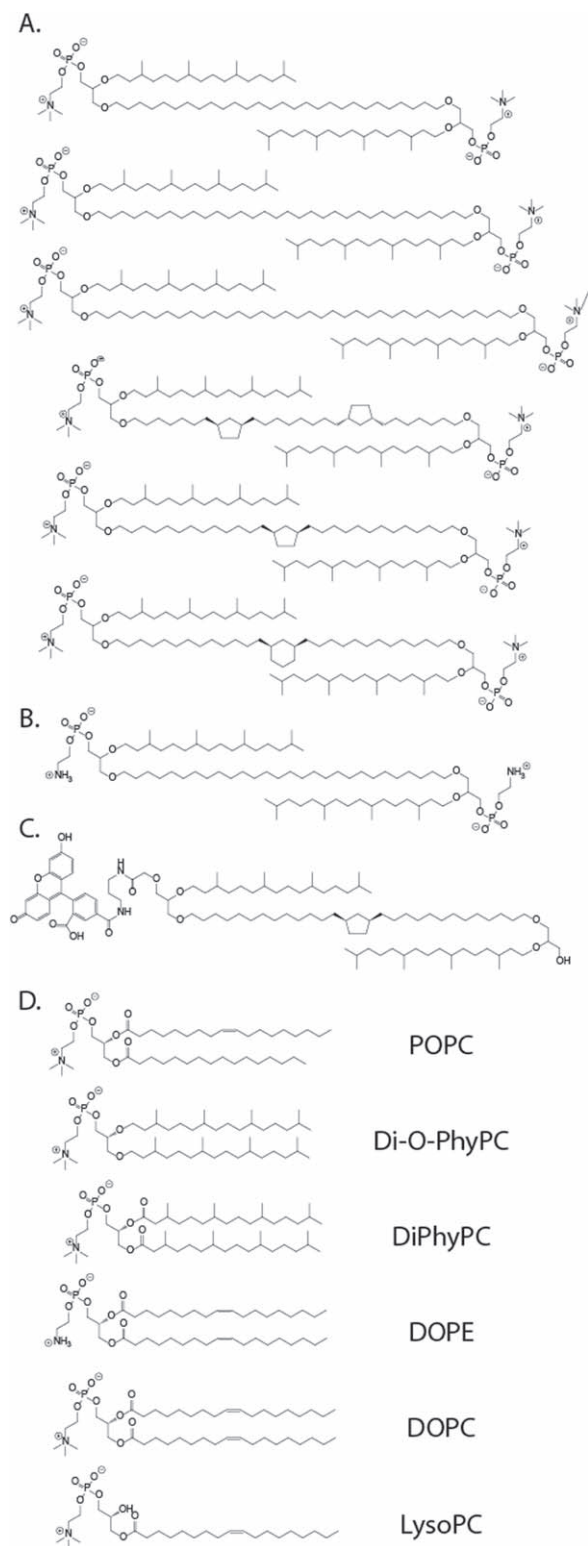


Figure 1. Chemical structures of all the lipids tested in this study. (A) Various archaea-inspired, monolayer-forming lipids. (B) Archaea-inspired lipid with a head group bearing a primary amine group for anchoring proteins. (C) Fluorescently-labeled archaea-inspired lipid. (D) All bilayer-forming lipids used in this work.

nanopores with extremely small radii of curvature. In order to enhance the coating's ability to conform to highly curved surfaces, we chose a 'curvature-tolerant' lipid composition containing lipids with a cone-shaped geometry (1-oleoyl-2-hydroxy-sn-glycero-3-phosphocholine or LysoPC), with a complementary inverted cone shape (1,2-dioleoyl-sn-glycero-3-phosphoethanolamine or DOPE), and with 1,2-dioleoyl-sn-glycero-3-phosphocholine (DOPC), a cylindrically shaped lipid [72].

2. Results and discussion

2.1. Baseline quality: noise and stability

Figure 2 shows that coating a nanopore with a lipid membrane had only a relatively small effect on the noise in the most important frequency range, above 5 kHz for most lipid compositions, as reflected in the power spectra (distributions of noise power versus frequency, figures 2(B)–(D)). In contrast, lipid coating increased mostly the noise present in current recordings in the low frequency range ($1/f$ noise) [47]. Figure 2(A) shows plots of the root mean square (rms) current noise after coating a nanopore chip divided by the rms noise before coating a chip with lipid membranes of various compositions. Bilayer coatings of the phytanyl-bearing lipids DiPhyPC and Di-O-PhyPC produced the largest increase in noise, likely due to unruptured liposomes near the pore entrance, shown in figure 3. Curvature-tolerant lipid bilayers also significantly increased the noise in current recordings. These elevated noise levels putatively stem from the diversity of lipid shapes present in the bilayer. Given that membranes containing conical lipids are prone to forming curved regions [73], membrane undulations along the pore walls are likely more pronounced when the membrane is a mixture of curvature-tolerant lipids compared to membranes from non-conical lipids.

Increasing the proportion of cholesterol in POPC membranes had no significant effect on the noise; in general lipid coatings of pure POPC with 10 to 40 mol% cholesterol showed the smallest increase in noise upon coating with a tendency towards the lowest noise values with 20 mol% cholesterol. These favorable noise properties (figures 2(A) and (C)) are likely due to the structural changes cholesterol imparts to lipid membranes [57, 74]: since the addition of cholesterol improves the packing of membranes, cholesterol-doped membranes may be more stable and fluctuate less than in the absence of cholesterol. Overall, we observed the lowest noise recordings with coatings from POPC-cholesterol mixtures and from archaea-inspired lipid membranes that contained 80 to 100 area% of archaea-inspired lipids. Comparing the various types of archaea-inspired lipids shown in figure 1(A), we observed no differences with respect to the noise and stability of nanopore coatings.

With most of the lipid compositions tested here, the current baseline measured from lipid-coated nanopores was stable for the average duration of a protein translocation experiment (around one hour). Experiment-ending instability

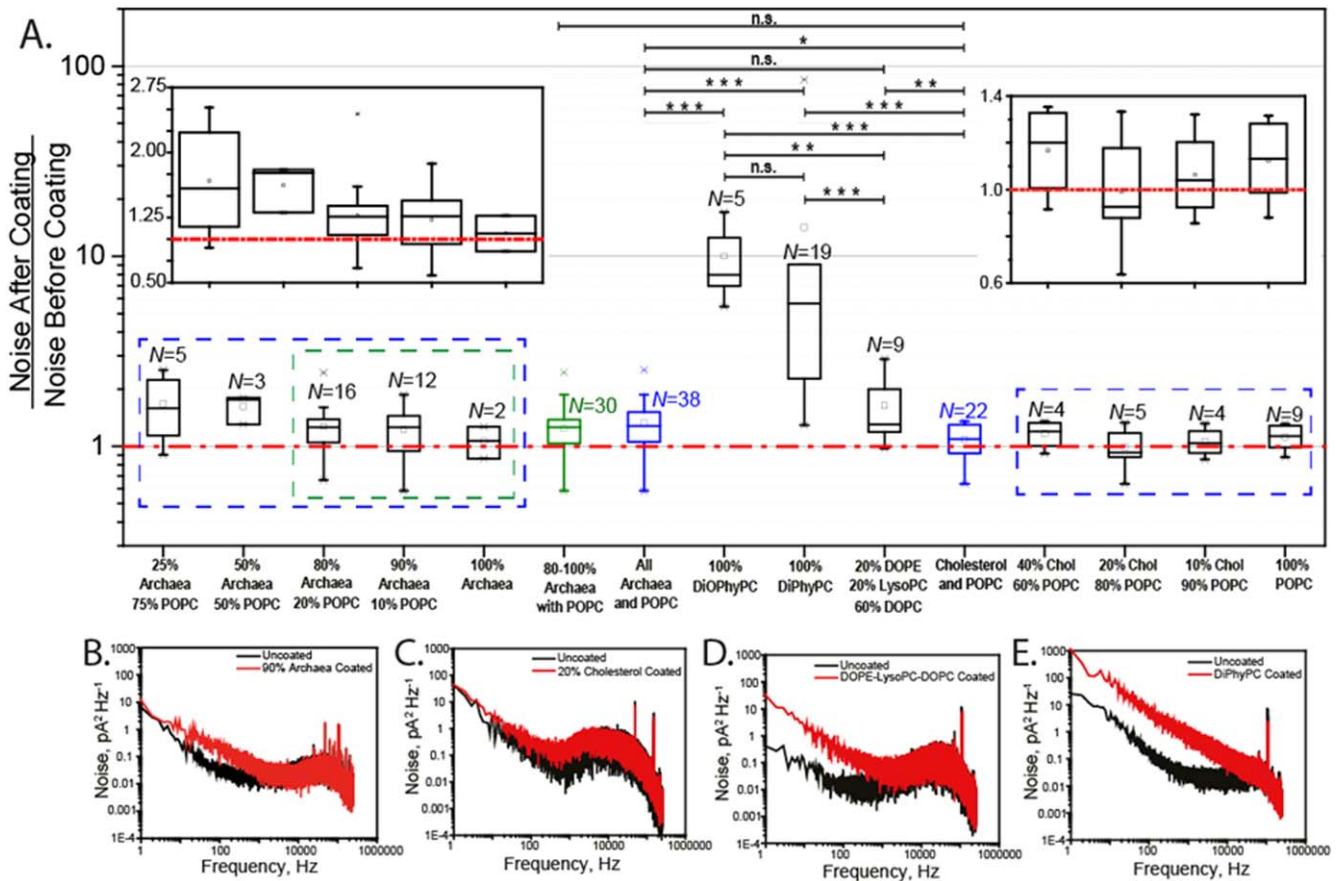


Figure 2. Ratio between the rms current noise after and before lipid coating of solid-state nanopore chips and power spectra of the recorded current for different membrane compositions. All rms noise values were determined after applying a digital Gaussian low-pass filter with a cutoff frequency of 15 kHz, while power spectra were determined from recordings with an effective bandwidth of ~ 55 kHz and a sampling rate of 500 kHz with -100 mV applied potential. (A) Ratio between the rms noise after and before lipid coating for all major lipid compositions studied. The lower whiskers reach to the outermost data points that fall within the lower inner fence, defined as the 25th percentile $-(1.5 \times \text{interquartile range})$, the upper whiskers reach to the outermost data points that fall within the upper inner fence, defined as the 75th percentile $+(1.5 \times \text{interquartile range})$, the box encompasses the interquartile range, the line represents the median and the small square represents the mean. The box plots in blue on the left represent combined data from coatings with archaea-inspired lipids and, on the right, from coatings with POPC and varying amounts of cholesterol. The green box plot represents the noise ratios for 80–100 area% archaea-inspired lipids with POPC. Significant difference between lipid compositions, as determined by a Kruskal–Wallis test, are indicated by * for $p < 0.05$, ** for $p < 0.001$, *** for $p < 0.0001$ and n.s. for no significance. The red dashed line indicates no change in noise due to coating. The inset to the left shows, on a linear scale, the ratio between the noise after and before coating for archaea-inspired lipid membranes with varying proportions of POPC (in area%, see Materials and Methods). The inset to the right shows, on a linear scale, the ratio between the rms noise after and before lipid coating for POPC bilayers containing varying proportions (in mol%) of cholesterol. (B)–(E). Noise power as a function of frequency for single pores before (black) and after lipid coating (red). Coatings were composed of (B) 90 area% archaea-inspired lipids and 10 area% POPC, (C) 80 mol% POPC and 20 mol% cholesterol, (D) 20 mol% DOPE, 20 mol% LysoPC and 60 mol% DOPC and (E) pure DiPhyPC.

was rare, and when it did occur, it generally began after the addition of protein. Lipid coatings made from DiPhyPC and Di-O-PhyPC bilayers were more prone to unstable baseline currents than coatings of other lipid compositions. Epifluorescence microscopy revealed that during the coating procedure with these two lipids, many small unilamellar vesicles (SUVs) did not burst despite the osmotic pressure gradient. The resulting surface-attached residual SUVs likely contributed to baseline fluctuations due to the proximity of these liposomes to the nanopore entrance. Figure 3(A) displays a fluorescent image of a well-coated nanopore made with liposomes from POPC lipids, with the corresponding stable current trace in figure 3(B). In contrast, figure 3(C) shows a fluorescent image of liposomes from DiPhyPC lipids

on the chip window with the corresponding unstable current trace in figure 3(D).

2.2. Lateral diffusion of lipids

Figure 4 shows D_L values obtained via fluorescence recovery after photobleaching (FRAP) experiments that were carried out on the SiN_x membrane of nanopore chips after coating with various lipid compositions. The inset shows that D_L values of coatings from POPC lipids could be varied by a factor of ~ 3 by including 10 to 50 mol% of cholesterol in the lipid composition. Overall, the results in figure 4 show that D_L values measured in nanopore coatings composed of membrane-spanning archaea-inspired lipids were approximately

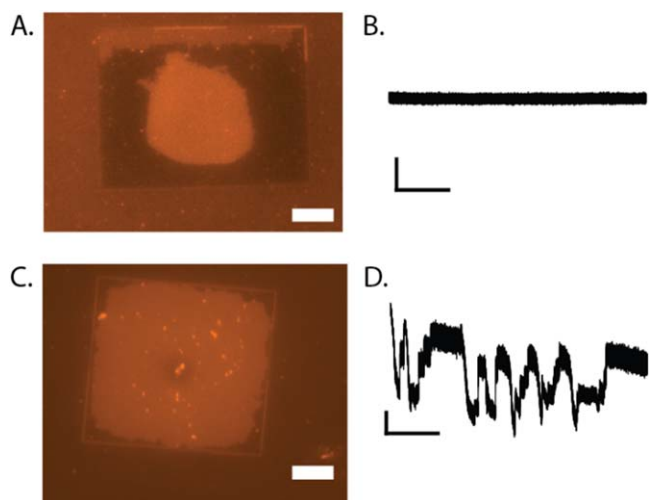


Figure 3. Epifluorescence microscopy images and corresponding current versus time recordings from nanopore chips with SiN_x membranes that were coated with POPC or DiPhyPC lipids. DiPhyPC (and Di-O-PhyPC) bilayers formed coatings with poor baseline stability. (A) Epifluorescence image of a pore coated with POPC lipids. (B) Representative current trace for a pore coated with POPC lipids. (C) Epifluorescence image showing unruptured liposomes on a nanopore chip coated with DiPhyPC lipids. (D) Representative current trace for a pore coated with a DiPhyPC bilayer. All lipid compositions contained 0.8 mol% Rhodamine-PE lipids; unruptured liposomes appear as bright spots. The scale bars on both images represent $20 \mu\text{m}$. The y -axis scale on the current traces represents 2 nA and the x -axis scale represents 2 s.

10-fold smaller than for the D_L of bilayers of pure POPC or DiPhyPC, DOPE and LysoPC. Because of their strongly increased viscosity, these monolayer-forming coatings from archaea-inspired lipids doubled the fraction of protein translocation events with dwell times longer than $400 \mu\text{s}$ compared to experiments with lipid membranes of pure POPC when we used the same relative amount of lipid anchor and protein. This high viscosity of coatings from archaea-inspired lipids also reduced the event frequency by a factor of approximately 10 compared to bilayer coatings at the same concentration of tethered protein and resulted in detectable event frequencies smaller than 1 Hz. Such low event frequencies pose two challenges: first, they lengthen the required duration of each experiment to collect a representative number of translocation events, thereby necessitating long-term stability of membrane coatings. Second, resistive pulses stemming from noise artifacts (which have a very low but non-negligible statistical likelihood [75]) during long recording times gain more influence over the population of collected events. To avoid impractically long durations of the experiments, the frequency of resistive pulses should range between 1 and 10 Hz, and hence the slow diffusion of lipid-anchored analytes should be compensated for by increasing the density of lipid anchors in the coating. For the experiments reported here, we used a fraction of 1 mol% of potential lipid anchors but a fraction of 10 mol% can be achieved with most anchors if desired.

To investigate whether the lipid tether or the overall lipid composition of the coating dominated the observed diffusion of lipid-anchored proteins, we used an archaea-inspired

membrane-spanning lipid to anchor translocating proteins in both bilayer-forming and monolayer-forming lipid compositions. To our surprise, lipid anchors from monolayer- or bilayer-forming lipids did not produce a significant difference in the event frequency or distribution of t_d values when compared to respective experiments that used a shorter, bilayer-forming lipid to anchor the proteins. In addition to t_d values, we also used FRAP experiments to compare the diffusion constants of fluorescently-labeled bilayer-forming and fluorescently-labeled monolayer-forming lipids both in a supported lipid membrane made from archaea-inspired monolayer-forming lipids and in a coating of bilayer-forming lipids. The resulting D_L values likewise were not significantly different as a function of the lipid to which the fluorophore was attached but rather depended on the viscosity of the respective overall lipid composition of the membrane. These results indicate that the background lipid composition defined the lateral diffusion of the tethered species. Figure 1 shows that we conducted experiments with six different archaea-inspired lipids. Results with regard to membrane viscosity were similar across this set of lipids [65], especially when compared to non-bolaamphiphilic lipid membranes, which is why we did not differentiate between different archaea-inspired lipids.

2.3. Ease of coating

During this investigation, we found that nanopores fabricated by ion beam sculpting produced stable coatings more frequently than nanopores fabricated by ion beam drilling or dielectric breakdown [50, 52]. None of the lipid compositions that we tested, including the curvature-tolerant lipid mixture, had a significant effect on the success rate or ease of coating. We found, however, that pores made by ion beam drilling or dielectric breakdown, which initially resisted coating, often could be coated more readily by all lipid compositions after ten or more cleaning cycles (see Materials and Methods). Since these cleaning cycles were frequently accompanied by an increase in the pore diameter as quantified from current measurements, we hypothesized that pores fabricated by these two methods initially contained rougher surfaces or sharper edges than those formed by ion beam sculpting and that these edges were smoothed over time by the slow surface etching induced by the cleaning solution or by the aqueous electrolyte during experiments [76].

In contrast, most of the nanopores that coated reliably well in this work were fabricated using an ion beam sculpting technique, in which He ions, which are directed towards a focused ion beam-drilled pore ($\sim 100 \text{ nm}$ diameter), cause the pore to shrink to a desired diameter through mass flow of silicon nitride [7]. Once the sculpting process was complete, each ion beam sculpted pore was temperature treated during an annealing process in an inert atmosphere [76]. Most of the pores produced by ion beam drilling or dielectric breakdown that were difficult to coat initially did not undergo annealing during production [52, 77]. Rollings *et al* [76] and we [50] have shown that annealing smoothens the shape at the rim of silicon nitride nanopores and that this effect likely renders

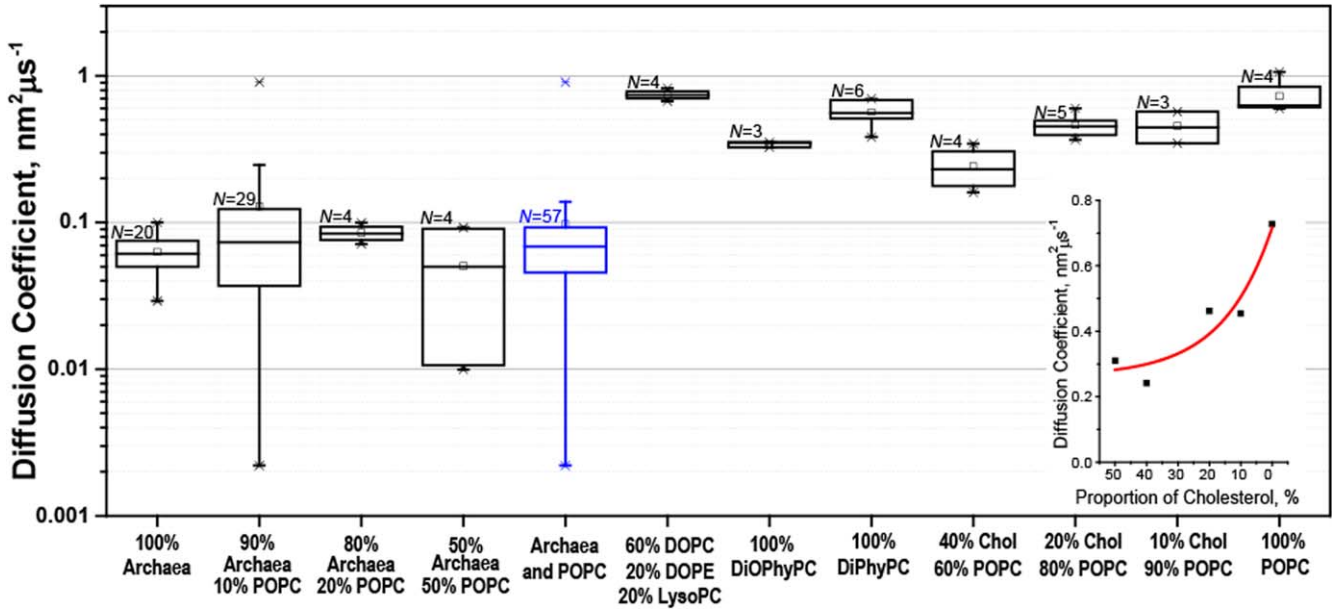


Figure 4. Box plots displaying the lateral diffusion coefficients D_L of all the major lipid compositions examined in this work as determined by FRAP on the SiN_x windows of nanopore chips. The lower whiskers reach to the outermost data points that fall within the lower inner fence, defined as the 25th percentile $-(1.5 \times \text{interquartile range})$, the upper whiskers reach to the outermost data points that fall within the upper inner fence, defined as the 75th percentile $+(1.5 \times \text{interquartile range})$, the box encompasses the interquartile range, the line represents the median and the small square represents the mean. The box plot in blue represents the combined data from coatings with archaea-inspired lipids and mol% for compositions containing only bilayer-forming lipids. The inset shows the mean values of the diffusion coefficient as a function of proportion of cholesterol in a bilayer of POPC lipids, the red curve represents a fit with $D_L (\text{in } \text{nm}^2 \mu\text{s}^{-1}) = 0.45 \text{ nm}^2 \mu\text{s}^{-1} \times e^{-\frac{X_{\text{Chol}} (\text{in mol}\%)}{15.9 \text{ mol}\%}} + 0.26 \text{ nm}^2 \mu\text{s}^{-1}$ where X_{Chol} is the proportion of cholesterol in the membrane.

nanopores amenable to coating with lipids. Rollings *et al* also demonstrated an increase in the stability towards slow etching in electrolyte solution of uncoated ion-beam sculpted pores after annealing, possibly due to a decrease in the number of dangling bonds left over from the fabrication process [76]. AFM images taken by Rollings and TEM images taken by us indeed indicated a smoother surface after annealing [50, 78]. Asghar *et al* showed that annealing also alleviates residual stress in silicon oxide nanopores [79]. We hypothesized that these effects together may have increased the success rates for generating lipid coatings of high quality. This hypothesis is supported by the observation that pores formed by controlled dielectric breakdown [55, 80, 81] initially were difficult to coat, while an annealing step doubled the success rate of coating and improved the noise characteristics in both uncoated and coated states [50]. Altogether, these results indicate that pore morphology is a critical parameter for the success of coating nanopore chips with lipid membranes.

2.4. Determining protein charge

One major advantage of coating nanopore walls with fluid lipid coatings is that this approach makes it possible to slow down the translocation of proteins by means of attaching them to a lipid anchor. The viscous drag of this anchor slows down the translocation of tethered proteins by two orders of magnitude, making it possible to resolve complete distributions of translocation times, t_d . These t_d distributions reveal the net charge of the protein by fitting the distribution to the equation

for a biased first-passage time process [16, 45]:

$$P(t_d) = \frac{l_p}{\sqrt{4\pi D_L t_d^3}} e^{-(l_p - vt_d)^2 / 4D_L t_d}, \quad (1)$$

where $v = |z|eV_p D_L / l_p k_B T$. The parameter $|z|$ (unitless) represents the net number of unit charges carried by the protein, V_p (V) is the drop in electrical potential across the nanopore, k_B (J K^{-1}) is the Boltzmann constant and T (K) is the temperature of the system. This approach assumes that the lateral diffusion coefficient of the lipid anchor with the attached protein is the same as the average D_L value of the lipids in the bilayer coating [16].

For charge determination in previous work [15, 16], we have typically fit the experimentally-determined probability distribution of t_d values with equation (1). However, when we applied this approach to data from experiments with nanopore coatings from archaea-inspired lipids, the determined charge values were unrealistically high and the model could not fit the data (with adjusted R^2 values < 0.5 in all cases). Close inspection of the recorded t_d data revealed a large population of short dwell times ($< 40 \mu\text{s}$) that dominated the distribution and were too short to originate from proteins that were lipid-anchored to a highly viscous coating from archaea-inspired lipids. We hypothesized that this first population of short translocation times primarily represented false events due to fluctuations in the baseline noise [75] and proteins that have lost their lipid tether during the course of the experiment.

Table 1. Comparison of the lipid compositions tested with regard to their suitability for resistive pulse recordings based on four characteristics.

Lipid composition of coating	Stable baseline	Low noise	Slow translocation	Straightforward to coat
100% POPC	+	+	+	+
25, 50, 80, 90, 100% archaea Lipids + 75, 50, 20, 10, 0% POPC	+	+	++	+
100% DiPhyPC	--	--	+	+
100% Di-O-PhyPC	--	--	+	+
60% DOPC + 20% DOPE + 20% LysoPC	+	-	+	+
10, 20, 0, 40% Cholesterol +90, 80, 70, 60% POPC	+	+	+	+
50% Cholesterol + 50% POPC	+	+	+	-

++ Indicates that a coating performed very well, + indicates that a coating performed well, - represents a negative influence as a result of this coating and -- is for a very negative influence. All percentage values are in area% for compositions containing archaea-inspired lipids and mol% for compositions containing bilayer-forming lipids.

To account for these artifacts, we first integrated equation (1) to obtain the cumulative density function (CDF). This change allowed us to perform fitting on the data without the influence of binning. Next, we expanded the CDF to allow for the fitting of three separate populations within the cumulative distribution of measured t_d values. This expansion of the fitting equation made it possible to account for (1) the first population of t_d values shorter than 40 μ s that we attributed to artifacts, (2) an intermediate population with the range of expected t_d values, and (3) a small, third population with dwell times longer than 1 ms, representing events of a few proteins that may have interacted non-specifically with the pore. We then determined the charge of three different proteins from the fit to the 2nd population in the middle of the distribution, resulting in mean charge values within $\pm 30\%$ of reference values (see figure S1, available online at stacks.iop.org/NANO/30/325504/mmedia) [15]. Further details on the integration of equation (1) and the function for three-population fits can be found in the Supplementary Information.

3. Conclusions

Table 1 summarizes the conclusions from this investigation. By the quality criteria discussed here, we recommend either coatings from either pure POPC or with 10–20 mol% cholesterol or coatings from either pure archaea-inspired lipids or with 10–20 area% POPC for optimal nanopore-based characterization. Among these, the monolayer-forming lipids inspired by archaea led to the longest translocation times of all the lipids tested while maintaining stable, low-noise baselines. The low event frequency as a consequence of the high viscosity of these monolayer coatings can be addressed by increasing the proportion of lipid anchors in the coating and the accumulation of short-lived, false translocation events from statistical baseline fluctuations over extended recording times [75] can be minimized by restricting the analysis only to events with dwell times $>40 \mu$ s through multiple-population fitting. We further recommend annealing of nanopore chips (regardless of fabrication method) to improve their stability in aqueous electrolytes as well as their ability to support a lipid membrane coating.

4. Materials and methods

We obtained all non-bolaform phospholipids from Avanti Polar Lipids. We synthesized archaea-inspired lipids as described by Koyanagi *et al* [63–67]. We purchased L-lactate dehydrogenase (59747) from Sigma Aldrich. We purchased polyclonal anti-biotin IgG-Fab fragments (800-101-098) from Rockland.

Unless specified otherwise, we performed protein translocation experiments using silicon chips containing 275 nm thick, 30 μ m \times 30 μ m silicon nitride windows, each bearing one nanopore, sculpted by a focused ion beam, as described by Li *et al* [7]. The narrowest constriction of these ion beam sculpted pores had a length of 10–30 nm with diameters ranging from 25–45 nm and a pore shape that can be approximated by a cylinder [15]. This nanopore opens up to a channel that is approximately 265 nm long. The channel is roughly cylindrical, expanding within a few nanometers from the pore to a diameter of about 100 nm. In addition to these chips, we used nanopores prepared by drilling with a He ion beam, as described by Yang *et al* [54]. These pores had a length of 20 nm with diameters ranging from 25–40 nm and a slight hourglass-like geometry [53]. As the third type of nanopore, we fabricated pores by dielectric breakdown using a modified procedure based on the one first described by Kwok *et al* [55]. Specifically, we enlarged the diameter of the nanopore slowly to 20 nm by applying a bipolar electric field with reduced amplitude that resulted in a cylindrically shaped pore [50].

We performed annealing as described by Rollings *et al* [76] by heating the chips in an inert nitrogen atmosphere over the course of 1 h from room temperature to 700 $^{\circ}$ C, holding the chips at this temperature for 30 min and letting them cool overnight to room temperature.

Before experiments, the nanopores were cleaned in freshly mixed, hot piranha solution (3:1 (v/v) concentrated sulfuric acid and 30% (v/v) aqueous hydrogen peroxide), rinsed copiously with deionized water and dried with N_2 gas.

During each experiment, we coated the freshly piranha cleaned nanopore substrates with a supported lipid membrane by depositing and fusing small unilamellar vesicles (SUVs) composed of the appropriate lipid composition onto the

silicon nitride substrate as described by Yusko *et al* [16]. Almost all lipid compositions included 0.8 mol% rhodamine PE lipids for fluorescence microscopy and FRAP analysis; with the exception of several experiments performed using a fluorescein-tagged archaea-inspired lipid (figure 1(C)). Briefly, we formed lipid coatings by filling the upper compartment of the PDMS-nanopore setup with aqueous solution (150 mM KCl buffered at pH 7.4 with 10 mM HEPES) containing the SUVs (lipid concentration of 2 mM) and added the same buffer without SUVs to the bottom compartment. After an incubation period of 20 min, we rapidly immersed the entire setup in a large (≥ 500 ml) beaker of deionized water to favor bursting of residual liposomes by the resulting osmotic pressure gradient and to remove excess liposomes. We replaced the buffer with 2 M KCl containing either 10 mM HEPES buffer, pH 7.4 for experiments with Fab or 10 mM potassium citrate, pH 6.1 for experiments with L-lactate dehydrogenase.

In the case of membrane-spanning, monolayer-forming, archaea-inspired lipids, we quantified the proportion of lipids as area% instead of mol% because from the point of view of the lipid coating that is exposed towards the lumen of the pore, the relevant parameter is what proportion of the exposed area is composed of archaea-inspired lipids and what proportion is composed of bilayer-forming lipids. This approach assumes that the area per lipid of a membrane-spanning archaea-inspired lipid with a PC headgroup is the same as the area per lipid of a bilayer-forming lipid with a PC head group. Hence, for the membrane-spanning archaea-inspired lipids used here, a membrane with 80 area% archaea-inspired lipids and 20 area% POPC lipids corresponds to a membrane with 40 mol% archaea-inspired lipids and 60 mol% POPC lipids.

To confirm that each nanopore had successfully acquired a lipid coating, we used at least two methods: (1) comparing pre- and post-coating resistance values of the nanopore to the expected theoretical values [15, 16, 50] and (2) inspecting the fluorescence intensity by epifluorescence microscopy (as described in Yusko *et al* [16]). Because the addition of a lipid membrane decreases the nanopore diameter and increases the nanopore length, the current value observed under a constant voltage decreases by a predictable extent after coating and the fluorescence intensity typically increases in the area of the nanopore chip with the nanopore where a lipid membrane covers the top and bottom [16]. The most stringent quality criterion of lipid coatings, however, was provided by fits to translocation time distributions. Only high quality coatings make it possible to determine protein charge by fitting these data to the equation for a biased first-passage time process [15, 16].

We used a Nikon E600FN upright microscope equipped with an X-cite 120 Fluorescence Illumination System and a CoolSnap HQ camera (Photometrics) and a 60 \times water-dipping objective (NA = 1.00) to image the lipid coatings and perform FRAP [16].

We measured rms noise properties from the standard deviation of the measured electrical baseline current at an applied potential of ± 100 mV after applying a digital

Gaussian low pass filter with a cutoff frequency of 15 kHz to the recorded current trace.

We anchored proteins to the lipid membrane in two ways: for anti-biotin Fab fragments we employed 0.15 mol% of a lipid that presented a biotin-group as its headgroup in the membrane (1 area% for membranes composed of archaea-inspired lipids). We attached the other proteins with bis(succinimidyl) penta(ethylene glycol), an amine-reactive crosslinker (Thermo Scientific, 21581), by reacting this crosslinker with 1 mol% lipids with an ethanolamine headgroup within the membrane coating [15]. Specifically, we dissolved the crosslinker in a 2 M KCl buffer containing 100 mM KHCO_3 at pH 8.4 and added the solution to the top of a lipid-coated nanopore chip at a final crosslinker concentration of 10 mg ml $^{-1}$. After 10 min incubation, we thoroughly rinsed away the crosslinker and added L-lactate dehydrogenase dissolved in the same carbonate buffer at the highest possible final protein concentration (between 1 and 3 μM). After at least 30 min, we rinsed away the excess protein and began recording with the specified recording buffer.

We performed protein sensing experiments as described by Yusko *et al* [15]. We measured current traces using Ag/AgCl pellet electrodes (Warner Instruments) with a patch-clamp amplifier (Axopatch 200B, Molecular Devices) at constant applied voltage of -100 mV. The buffer-filled compartment on the top was connected to the headstage of the amplifier and the bottom compartment was connected to ground. The analog low-pass filter of the amplifier was set to a cutoff frequency of 100 kHz. We acquired and stored data using a multifunction I/O device (PCI 6281, National Instruments) with a 500 kHz sampling frequency along with a custom LabView (National Instruments) program. All protein translocation analysis was performed using MATLAB (Mathworks). We first digitally filtered the data with a Gaussian 15 kHz low-pass filter and then applied a peak-finding algorithm developed by Pedone *et al* [82] to select regions of each current versus time recording where the measured current was greater than five times the standard deviation of the baseline current. The end of a resistive pulse was defined as the moment when the current returned to within one standard deviation of baseline current. We defined dwell times as the full-width at half-maximum value of the resistive pulse.

Acknowledgments

We thank J Golovchenko's Nanopore Group at Harvard University for the preparation of FIB pores. Research reported in this publication was supported by Oxford Nanopore Technologies (M.M., Grant No. 350509-N016133), the Swiss National Science Foundation (SNSF Grant No. 200021_169304 to M.M.), and a Graduate Research Fellowship from the National Science Foundation of the USA (JH).

ORCID iDs

Olivia M Eggenberger  <https://orcid.org/0000-0003-1426-9062>
 Cuifeng Ying  <https://orcid.org/0000-0002-7279-1388>
 Jared Houghtaling  <https://orcid.org/0000-0003-1557-9716>

References

- [1] Haque F, Li J, Wu H-C, Liang X-J and Guo P 2013 Solid-state and biological nanopore for real-time sensing of single chemical and sequencing of DNA *Nano Today* **8** 56–74
- [2] Branton D *et al* 2008 The potential and challenges of nanopore sequencing *Nat Biotech* **26** 1146–53
- [3] Venkatesan B M and Bashir R 2011 Nanopore sensors for nucleic acid analysis *Nat Nano* **6** 615–24
- [4] Li J L, Gershow M, Stein D, Brandin E and Golovchenko J A 2003 DNA molecules and configurations in a solid-state nanopore microscope *Nat. Mater.* **2** 611–5
- [5] Storm A J, Storm C, Chen J, Zandbergen H, Joanny J and Dekker C 2005 Fast DNA translocation through a solid-state nanopore *Nano Lett.* **5** 1193–7
- [6] Schneider G F, Kowalczyk S W, Calado V E, Pandraud G, Zandbergen H, Vandersypen L M K and Dekker C 2010 DNA translocation through graphene nanopores *Nano Lett.* **10** 3163–7
- [7] Li J, Stein D, McMullan C, Branton D, Aziz M J and Golovchenko J A 2001 Ion-beam sculpting at nanometre length scales *Nature* **412** 166–9
- [8] Gu L-Q and Shim J W 2010 Single molecule sensing by nanopores and nanopore devices *Analyst* **135** 441–51
- [9] Howorka S and Siwy Z 2009 Nanopore analytics: sensing of single molecules *Chem. Soc. Rev.* **38** 2360–84
- [10] Movileanu L 2009 Interrogating single proteins through nanopores: challenges and opportunities *Trends Biotechnol.* **27** 333–41
- [11] Dekker C 2007 Solid-state nanopores *Nat Nano* **2** 209–15
- [12] Shi W, Friedman A K and Baker L A 2017 Nanopore sensing *Anal. Chem.* **89** 157–88
- [13] Wanunu M and Meller A 2007 Chemically modified solid-state nanopores *Nano Lett.* **7** 1580–5
- [14] Hou X, Guo W and Jiang L 2011 Biomimetic smart nanopores and nanochannels *Chem. Soc. Rev.* **40** 2385–401
- [15] Yusko E C *et al* 2017 Real-time shape approximation and fingerprinting of single proteins using a nanopore *Nat Nano* **12** 360–7
- [16] Yusko E C, Johnson J M, Majd S, Prangko P, Rollings R C, Li J, Yang J and Mayer M 2011 Controlling protein translocation through nanopores with bio-inspired fluid walls *Nat Nano* **6** 253–60
- [17] Houghtaling J, List J and Mayer M 2018 Nanopore-based, rapid characterization of individual amyloid particles in solution: concepts, challenges, and prospects *Small* **14** 1802412
- [18] Quick J *et al* 2016 Real-time, portable genome sequencing for Ebola surveillance *Nature* **530** 228–32
- [19] Hurley J 1970 Sizing particles with a coulter counter *Biophys. J.* **10** 74–9
- [20] Uram J D, Ke K, Hunt A J and Mayer M 2006 Label-free affinity assays by rapid detection of immune complexes in submicrometer pores *Angew. Chem. Int. Ed.* **45** 2281–5
- [21] Uram J D, Ke K, Hunt A J and Mayer M 2006 Submicrometer pore-based characterization and quantification of antibody–virus interactions *Small* **2** 967–72
- [22] Han A, Schürmann G, Mondin G, Bitterli R A, Hegelback N G, de Rooij N F and Stauffer U 2006 Sensing protein molecules using nanofabricated pores *Appl. Phys. Lett.* **88** 093901
- [23] Bhakdi S and Tranum-Jensen J 1991 Alpha-toxin of staphylococcus aureus *Microbiol. Rev.* **55** 733–51
- [24] Braha O *et al* 1997 Designed protein pores as components for biosensors *Chem. Biol.* **4** 497–505
- [25] Nakane J J, Akesson M and Marziali A 2003 Nanopore sensors for nucleic acid analysis *J. Phys.: Condens. Matter.* **15** R1365
- [26] Jovanovic-Taliman T *et al* 2009 Artificial nanopores that mimic the transport selectivity of the nuclear pore complex *Nature* **457** 1023–7
- [27] Miles B N *et al* 2012 Single molecule sensing with solid-state nanopores: novel materials, methods, and applications *Chem. Soc. Rev.* **42** 15–28
- [28] Kececi K, Sexton L T, Buyukserin F and Martin C R 2008 Resistive-pulse detection of short dsDNAs using a chemically functionalized conical nanopore sensor *Nanomedicine* **3** 787–96
- [29] Li X *et al* 2016 Non-sticky translocation of bio-molecules through Tween 20-coated solid-state nanopores in a wide pH range *Appl. Phys. Lett.* **109** 143105
- [30] Tan S, Wang L, Liu H, Wu H and Liu Q 2016 Single nanoparticle translocation through chemically modified solid nanopore *Nanoscale Res. Lett.* **11** 50
- [31] Wang G, Zhang B, Wayment J R, Harris J M and White H S 2006 Electrostatic-gated transport in chemically modified glass nanopore electrodes *J. Am. Chem. Soc.* **128** 7679–86
- [32] Iqbal S M, Akin D and Bashir R 2007 Solid-state nanopore channels with DNA selectivity *Nat Nano* **2** 243–8
- [33] Lee S B and Martin C R 2001 pH-switchable, ion-permeable gold nanotubule membrane based on chemisorbed cysteine *Anal. Chem.* **73** 768–75
- [34] Wei R, Gatterdam V, Wieneke R, Tampé R and Rant U 2012 Stochastic sensing of proteins with receptor-modified solid-state nanopores *Nat Nano* **7** 257–63
- [35] Sexton L T *et al* 2007 Resistive-pulse studies of proteins and protein/antibody complexes using a conical nanotube sensor *J. Am. Chem. Soc.* **129** 13144–52
- [36] Chen P *et al* 2004 Atomic layer deposition to fine-tune the surface properties and diameters of fabricated nanopores *Nano Lett.* **4** 1333–7
- [37] Wang C *et al* 2015 Atomic layer deposition modified track-etched conical nanochannels for protein sensing *Anal. Chem.* **87** 8227–33
- [38] Hu R *et al* 2016 Intrinsic and membrane-facilitated α -synuclein oligomerization revealed by label-free detection through solid-state nanopores *Sci. Rep.* **6** 20776
- [39] Umehara S, Karhanek M, Davis R W and Pourmand N 2009 Label-free biosensing with functionalized nanopipette probes *Proc. Natl Acad. Sci.* **106** 4611–6
- [40] Kohli P *et al* 2004 DNA-functionalized nanotube membranes with single-base mismatch selectivity *Science* **305** 984–6
- [41] Ali M, Neumann R and Ensinger W 2010 Sequence-specific recognition of DNA oligomer using peptide nucleic acid (PNA)-modified synthetic ion channels: PNA/DNA hybridization in nanoconfined environment *ACS Nano* **4** 7267–74
- [42] Umehara S *et al* 2006 Current rectification with poly-l-lysine-coated quartz nanopipettes *Nano Lett.* **6** 2486–92
- [43] Schneider G F *et al* 2013 Tailoring the hydrophobicity of graphene for its use as nanopores for DNA translocation *Nat. Commun.* **4** 2619
- [44] Houghtaling J, Ying C, Eggenberger O M, Fennouri A, Nandivada S, Acharjee M, Li J, Hall A R and Mayer M 2019 Estimation of shape, volume, and dipole moment of individual proteins freely transiting a synthetic nanopore *ACS Nano* unpublished (<https://doi.org/10.1021/acsnano.8b09555>)

- [45] Ling D Y and Ling X S 2013 On the distribution of DNA translocation times in solid-state nanopores: an analysis using Schrödinger's first-passage-time theory *J. Phys.: Condens. Matter* **25** 375102
- [46] Sackmann E 1996 Supported membranes: scientific and practical applications *Science* **271** 43–8
- [47] Uram J D, Ke K and Mayer M 2008 Noise and bandwidth of current recordings from submicrometer pores and nanopores *ACS Nano* **2** 857–72
- [48] Plesa C *et al* 2013 Fast translocation of proteins through solid state nanopores *Nano Lett.* **13** 658–63
- [49] Yusko E C *et al* 2012 Single-particle characterization of A β oligomers in solution *ACS Nano* **6** 5909–19
- [50] Ying C, Houghtaling J, Eggenberger O M, Guha A, Nirmalraj P, Awasthi S, Tian J and Mayer M 2018 Formation of single nanopores with diameters of 20–50 nm in silicon nitride membranes using laser-assisted controlled breakdown *ACS Nano* **12** 11458–70
- [51] Stein D M, McMullan C J, Li J and Golovchenko J A 2004 Feedback-controlled ion beam sculpting apparatus *Rev. Sci. Instrum.* **75** 900–5
- [52] Marshall M M, Yang J and Hall A R 2012 Direct and transmission milling of suspended silicon nitride membranes with a focused helium ion beam *Scanning* **34** 101–6
- [53] Sawafita F, Carlsen A T and Hall A R 2014 Membrane thickness dependence of nanopore formation with a focused helium ion beam *Sensors* **14** 8150–61
- [54] Yang J *et al* 2011 Rapid and precise scanning helium ion microscope milling of solid-state nanopores for biomolecule detection *Nanotechnology* **22** 285310
- [55] Kwok H, Briggs K and Tabard-Cossa V 2014 Nanopore fabrication by controlled dielectric breakdown *PLoS ONE* **9** e92880
- [56] Senior J and Gregoriadis G 1982 Stability of small unilamellar liposomes in serum and clearance from the circulation: the effect of the phospholipid and cholesterol components *Life Sci.* **30** 2123–36
- [57] Meyer F de and Smit B 2009 Effect of cholesterol on the structure of a phospholipid bilayer *Proc. Natl Acad. Sci.* **106** 3654–8
- [58] Crane J M and Tamm L K 2004 Role of cholesterol in the formation and nature of lipid rafts in planar and spherical model membranes *Biophys. J.* **86** 2965–79
- [59] Sullan R M A, Li J K, Hao C, Walker G C and Zou S 2010 Cholesterol-dependent nanomechanical stability of phase-segregated multicomponent lipid bilayers *Biophys. J.* **99** 507–16
- [60] Filippov A, Orädd G and Lindblom G 2003 The effect of cholesterol on the lateral diffusion of phospholipids in oriented bilayers *Biophys. J.* **84** 3079–86
- [61] Albers S-V and Meyer B H 2011 The archaeal cell envelope *Nat. Rev. Microbiol.* **9** 414–26
- [62] Jacquemet A, Barbeau J, Lemiègre L and Benvegna T 2009 Archaeal tetraether bipolar lipids: structures, functions and applications *Biochimie* **91** 711–7
- [63] Koyanagi T *et al* 2016 Cyclohexane rings reduce membrane permeability to small ions in Archaea-inspired tetraether lipids *Angew. Chem. Int. Ed.* **55** 1890–3
- [64] Koyanagi T *et al* 2016 Effect of headgroups on small-ion permeability across Archaea-inspired tetraether lipid membranes *Chem. Eur. J.* **22** 8074–7
- [65] Schroeder T B H *et al* 2016 Effects of lipid tethering in extremophile-inspired membranes on H⁺/OH⁻ flux at room temperature *Biophys. J.* **110** 2430–40
- [66] Leriche G *et al* 2017 Characterization of drug encapsulation and retention in Archaea-inspired tetraether liposomes *Org. Biomolecular Chem.* **15** 2157–62
- [67] Koyanagi T, Cao K J, Leriche G, Onofrei D, Holland G P, Mayer M, Sept D and Yang J 2017 Hybrid lipids inspired by extremophiles and eukaryotes afford serum stable membranes with low leakage *Chem. Eur. J.* **23** 6757–62
- [68] White S H 1980 Small phospholipid vesicles: internal pressure, surface tension, and surface free energy *Proc. Natl Acad. Sci. USA* **77** 4048–50
- [69] Deserno M and Gelbart W M 2002 Adhesion and wrapping in colloid-vesicle complexes *J. Phys. Chem. B* **106** 5543–52
- [70] Roiter Y *et al* 2008 Interaction of nanoparticles with lipid membrane *Nano Lett.* **8** 941–4
- [71] Mornet S, Lambert O, Duguet E and Brisson A 2005 The formation of supported lipid bilayers on silica nanoparticles revealed by cryoelectron microscopy *Nano Lett.* **5** 281–5
- [72] Hamai C, Yang T, Kataoka S, Cremer P S and Musser S M 2006 Effect of average phospholipid curvature on supported bilayer formation on glass by vesicle fusion *Biophys. J.* **90** 1241–8
- [73] Israelachvili J N, Marcelja S and Horn R G 1980 Physical principles of membrane organization *Q. Rev. Biophys.* **13** 121–200
- [74] McIntosh T J 1978 The effect of cholesterol on the structure of phosphatidylcholine bilayers *Biochimica et Biophysica Acta (BBA)—Biomembranes* **513** 43–58
- [75] Rosenstein J K, Wanunu M, Merchant C A, Drndic M and Shepard K L 2012 Integrated nanopore sensing platform with sub-microsecond temporal resolution *Nat Meth* **9** 487–92
- [76] Rollings R *et al* 2015 The effects of geometry and stability of solid-state nanopores on detecting single DNA molecules *Nanotechnology* **26** 044001
- [77] Storm A J, Chen J H, Ling X S, Zandbergen H W and Dekker C 2003 Fabrication of solid-state nanopores with single-nanometre precision *Nat. Mater.* **2** 537–40
- [78] Rollings R 2013 The geometry and sensitivity of ion-beam sculpted nanopores for single molecule DNA analysis *Doctor of Philosophy in Physics* University of Arkansas
- [79] Asghar W, Ilyas A, Billo J A and Iqbal S M 2011 Shrinking of solid-state nanopores by direct thermal heating *Nanoscale Res. Lett.* **6** 372
- [80] Briggs K, Kwok H and Tabard-Cossa V 2014 Automated fabrication of 2-nm solid-state nanopores for nucleic acid analysis *Small* **10** 2077–86
- [81] Briggs K *et al* 2015 Kinetics of nanopore fabrication during controlled breakdown of dielectric membranes in solution *Nanotechnology* **26** 084004
- [82] Pedone D, Firmkes M and Rant U 2009 Data analysis of translocation events in nanopore experiments *Anal. Chem.* **81** 9689–94